Journal of Materials Chemistry A

ROYAL SOCIETY OF CHEMISTRY

PAPER

View Article Online
View Journal | View Issue

Check for updates

Cite this: J. Mater. Chem. A, 2025, 13, 4292

Organic-free synthesis of silicoaluminophosphate zeotype membranes with tunable framework charge density†

Sung Hwan Park, ‡[a] Bratin Sengupta,‡[a] Saman Emami Gerami, [a] Kaleb Friedman,[a] Rumwald Lecaros,[a] Amr F. M. Ibrahim [ab] and Miao Yu *[ac]

Received 19th September 2024
Accepted 20th December 2024

DOI: 10.1039/d4ta06666a

rsc.li/materials-a

Microporous crystalline membranes utilizing strong adsorptive affinity for separation, especially at elevated temperatures, are needed for separating mixtures containing polar and nonpolar molecules with similar sizes. Zeotype membranes with tunable framework charge densities (FCDs) may serve as a promising candidate for separating such mixtures under industrially relevant conditions. Typically, synthesis of zeotype membranes requires organic compounds as structure-directing agents (SDAs), increasing synthesis cost and complexity and thus potentially restricting their large-scale use. This work reports, for the first time, organic-free synthesis of silicoaluminophosphate (SAPO) zeotype membranes with LTA topology by secondary growth. By varying framework heteroatom (Si) concentrations, the FCD of LTA-type SAPO membranes was tuned between 0.30 and 0.37 with respect to charge-density matching with the inorganic SDA, Na^+ cation. Highly charged SAPO membranes showed good separation performance of ammonia (NH_3) over non-polar N_2 and H_2 gases, with selectivities of 32.5 and 9.9, respectively, and excellent thermal stability over 100 h at 150 °C. This inorganic synthesis strategy might be applicable to the fabrication of other types of zeotype membranes with adjustable compositions for affinity-based separations.

Open Access Article. Published on 03 January 2025. Downloaded on 2/9/2026 8:08:45 PM.
This article is licensed under a Creative Commons Attribution 3.0 Unported Licence.

1. Introduction

Membranes for separation under industrially relevant conditions, especially at elevated temperatures, can realize substantial energy savings.[1,2] Although polymers possess excellent processibility for membrane fabrication, they often suffer from a low degree of thermal stability, making them inapplicable for such separations.[3] Microporous inorganic materials, such as zeolites with molecular-sized pores, have exceptional thermal, mechanical and chemical stabilities and thus are promising alternatives for fabricating membranes for gas separation at high temperatures.[4–8]

Besides zeolites, a family of aluminophosphate ($AlPO_4$)-based molecular sieves, including heteroatom-substituted zeotypes, such as silicoaluminophosphate (SAPO) materials, have also been utilized for membrane fabrication.[8–12] For example, due to their limited availability in aluminosilicate zeolite systems, AEI- and AFI-type membranes have been fabricated from $AlPO_4$-18 and SAPO-5 zeotype materials and demonstrated potential for CO_2 and hydrocarbon separations using their small- and large-pore frameworks, respectively.[13–15] On the other hand, zeotype membranes often exhibit enhanced separation performance compared to zeolite membranes, even if they share the same framework topology. For example, SAPO-34 membranes, analogues of CHA-type zeolite membranes, have shown higher N_2 permeance compared to SSZ-13 membranes, making them more attractive in N_2 separation for the natural gas process.[16,17]

However, the synthesis of zeotype membranes usually requires the use of organic structure-directing agents (SDAs), such as alkylamines or organoammonium cations, either for seed-crystal preparation and/or secondary membrane growth,[8,11,12] despite many efforts toward template-free or gel-free membrane growth.[18–20] On the other hand, in the synthesis of low-silica (Si/Al ≤ 3) zeolite membranes, a smaller metal cation with higher charge density has been used as an inorganic SDA to introduce higher framework charge density (FCD), providing enhanced adsorption selectivity for polar molecules.[21,22] This, therefore, arouses great interest in developing a complete inorganic synthesis strategy for the fabrication of zeotype membranes, where high-charge-density inorganic SDAs would allow the introduction of a higher FCD within zeotype membranes, realizing more effectively controlled affinity-based separations. Moreover, this would

[a]Department of Chemical and Biological Engineering, University at Buffalo, Buffalo, NY 14260, USA. E-mail: myu9@buffalo.edu
[b]Faculty of Petroleum and Mining Engineering, Suez University, Suez 43512, Egypt
[c]RENEW Institute, University at Buffalo, Buffalo, NY 14260, USA

† Electronic supplementary information (ESI) available. See DOI: https://doi.org/10.1039/d4ta06666a

‡ These authors contributed equally to this work.

This journal is © The Royal Society of Chemistry 2025

Open Access Article. Published on 03 January 2025. Downloaded on 2/9/2026 8:08:45 PM.
This article is licensed under a Creative Commons Attribution 3.0 Unported Licence.

eliminate the energy intensive calcination step that is typically required for the synthesis of zeolitic materials using organic SDAs.

Herein, we report unprecedented organic-free synthesis of SAPO zeotype membranes using an alkali metal cation as an inorganic SDA, with relatively higher charge density compared to zeotype materials synthesized from organic SDAs. As the first analogue of commercial NaA zeolite membranes, we fabricated a series of small-pore (~4.5 Å) LTA-type SAPO (SAPO-LTA) membranes with highly charged frameworks whose FCD was effectively controlled by varying framework heteroatom distributions. We also demonstrated the high-temperature (up to 300 °C) application of these highly charged SAPO-LTA membranes for affinity-based separation of polar gas (NH_3) from similarly sized, non-polar gases (H_2 and N_2).

2. Experimental section

2.1 Preparation of SAPO-LTA molecular sieves

The reagents used for the synthesis of SAPO molecular sieves as seed crystals included NaOH (50%, Aldrich), aluminium hydroxide (99%, Aldrich), phosphoric acid (85%, Merck), Ludox AS-40 (40% colloidal silica in water, Aldrich), and de-ionized (DI) water. The oxide composition of the final synthesis mixture was $2.4Na_2O{\cdot}1.0Al_2O_3{\cdot}0.9P_2O_5{\cdot}xSiO_2{\cdot}yH_2O$, where x and y are varied between $2.0 \leq x \leq 3.0$ and $100 \leq y \leq 300$, respectively. All chemical reagents were mixed by high-speed stirring to prepare homogeneous synthesis gels. The prepared synthesis mixtures were heated at 135 °C for 1 day. The obtained solid product was washed with DI water and dried at 70 °C.

2.2 Synthesis of SAPO-LTA membranes

SAPO-LTA membranes were prepared on α-Al_2O_3 ceramic hollow fiber supports (Media and Process Technology Inc, outer diameter: 5.7 mm, average pore size: 0.4 μm, wall thickness: 1 mm, and length: 7 cm), *via* a hydrothermal secondary growth method.[1,8] The ceramic supports were first washed with DI water under sonication for 1 h. After drying the supports at 200 °C for 1 h, a tip of the cooled-down support was glazed at 1000 °C for 6 h. The one-end sealed alumina supports were then dip-coated with 2 wt% seeding solutions prepared using the synthesized SAPO-LTA seed crystals, followed by drying at 200 °C overnight. The hydrothermal secondary growth of SAPO-LTA membranes was carried out on the seeded supports using SAPO synthesis mixtures identical to those used for the corresponding seed crystal synthesis, at 135 °C for 1 day. The as-synthesized membranes were recovered after washing several times with DI water and dried for up to 24 h at room temperature.

2.3 Characterization of LTA-type SAPO seed crystals and SAPO-LTA membranes

The crystal topologies and crystallinity of the LTA-type SAPO materials were determined by powder X-ray diffraction (XRD) on a Rigaku Ultima IV diffractometer with Cu Kα radiation at 40 kV and 40 mA. Crystal morphologies and sizes were determined by Carl Zeiss AURIGA CrossBeam field-emission scanning electron microscopy (SEM). The cross-sectional thickness was determined using energy dispersive spectroscopy (EDS) using a Hitachi SU70 FESEM coupled with an Oxford EDS. The crystal size distributions of SAPO-LTA in the seeding solution were determined by dynamic light scattering (DLS, Malvern Panalytical Zetasizer Nano). Elemental analysis for Na, Al, P and Si of the seed crystals was conducted using a Jarrell-Ash Polyscan 61E inductively coupled plasma spectrometer in combination with a PerkinElmer 5000 atomic absorption spectrophotometer. Thermogravimetric and differential thermal analyses (TGA/DTA) were performed in air on a TA Instruments SDT 2960 thermal analyser at a heating rate of 5 °C min^{-1}. ^{29}Si Magic-Angle Spinning (MAS) Nuclear Magnetic Resonance (NMR) measurements were performed on a Bruker DRX500 spectrometer at a spinning rate of 20.0 kHz. The ^{29}Si MAS NMR spectra were recorded at a ^{29}Si frequency of 99.362 MHz with a $\pi/2$ rad pulse length of 4.0 μs, a recycle delay of 10 s, and an acquisition of about 5000 pulse transients. The ^{29}Si chemical shifts are referenced to TMS. ^{27}Al and ^{31}P MAS NMR measurements were also performed on a DRX500 spectrometer at a spinning rate of 21.0 kHz. The solid sample was dehydrated at 250 °C for 6 h under a dynamic vacuum of 10^{-3} torr. ^{27}Al and ^{31}P MAS NMR data were collected at 130 and 202 MHz with a $\pi/6$ rad pulse length of 1.0 and 3.0 μs, respectively. The ^{27}Al and ^{31}P chemical shifts are referenced to an $Al(H_2O)_6^{3+}$ solution and a H_3PO_4 solution, respectively. N_2 gas adsorption measurements at 77 K were conducted using a Micromeritics 3Flex system. NH_3 temperature-programmed desorption (NH_3-TPD) was performed on a flow-type, fixed bed apparatus combined with a mass spectrometer (OmniStar GSD 350, Pfeiffer Vacuum). 0.1 g of SAPO-LTA seed crystals were activated in flowing N_2 (50 sccm) at 250 °C for 4 h. Then, NH_3 was flowed over the samples at 150 °C for 30 minutes. Finally, NH_3-TPD was performed in flowing N_2 (20 sccm) from 150 to 700 °C with a temperature ramping rate of 10 °C min^{-1}. The detailed information on the material preparation and gas separation methods is available in the ESI.†

3. Results and discussion

The synthesis procedure of SAPO-LTA membranes is illustrated in Fig. 1. To fabricate SAPO membranes by seeded growth under entirely inorganic conditions, we first prepared sodium-SAPO synthesis gels that can be used for both seed-crystal synthesis and membrane growth. By using the gels with adjusted Si contents, SAPO-LTA crystals with varied FCD were synthesized as seed crystals. Subsequently, porous alumina supports (Fig. S1†, OD: 5.7 mm; pore size: 400 nm) were seeded by a dip-coating process with each crystal. After that, secondary growth of SAPO-LTA membranes on the seeded supports was conducted using the gels under the optimized crystallization conditions that can also yield the SAPO seed crystals, to effectively control the chemical compositions of the resulting membranes with FCD corresponding to those of the seeds.

Because the secondary growth of zeolitic membranes involves seeded crystallization along a thin layer of targeted

Open Access Article. Published on 03 January 2025. Downloaded on 2/9/2026 8:08:45 PM.
This article is licensed under a Creative Commons Attribution 3.0 Unported Licence.

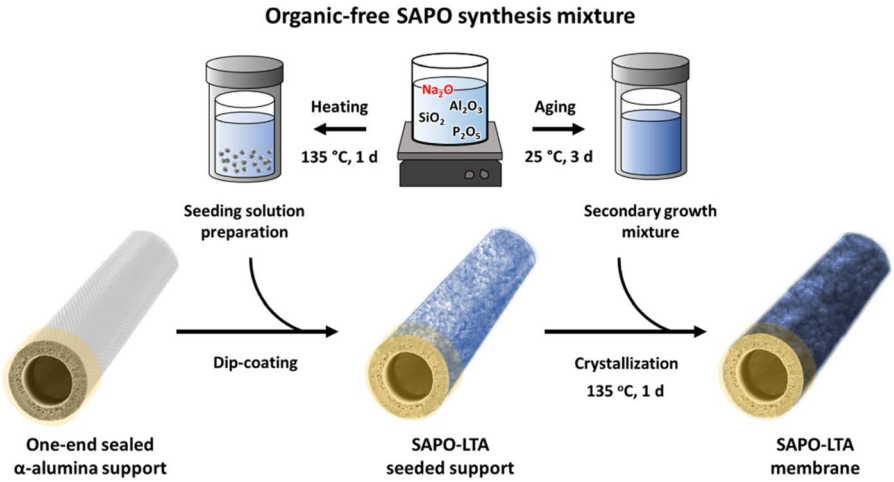

Fig. 1 Schematic illustration of the synthesis procedure for organic-free SAPO-LTA membranes *via* secondary growth.

zeolite seeds, a uniform deposition of nano-sized seed crystals on the substrate is required to improve the resulting membrane quality.[6–8] Therefore, our initial attempt at SAPO-LTA membrane fabrication was made with the synthesis of SAPO-LTA crystals of such small sizes (Table S1†). According to the previously known synthesis system for organic-free Na-SAPO-LTA molecular sieves,[23] indeed, we were only able to obtain micron-sized SAPO-LTA crystals (≥1 μm) from Na-SAPO gels with the composition of $2.4Na_2O{\cdot}1.0Al_2O_3{\cdot}0.9P_2O_5{\cdot}(2.0–2.5)SiO_2{\cdot}100H_2O$ (Fig. S2†). However, when the gels with a wider range of SiO_2/Al_2O_3 ratios (x = 2.0–3.0) were further diluted (H_2O/Al_2O_3 = 300), we could synthesize phase-pure LTA-type SAPO crystals (denoted as SAPO-LTA-x) (Fig. 2a) as small as ~500 nm (Fig. 2b and S2†), with the aid of a small addition (4 wt% Al_2O_3) of the micron-sized SAPO-LTA into the diluted gels (Table S1†). In fact, a crystallization time of 1 day at 135 °C for the synthesis of nano-sized SAPO-LTA as seed crystals was carefully selected for the maximum crystallinity of products observed from the crystallization kinetics (Fig. S3†). This further allowed us to determine secondary membrane

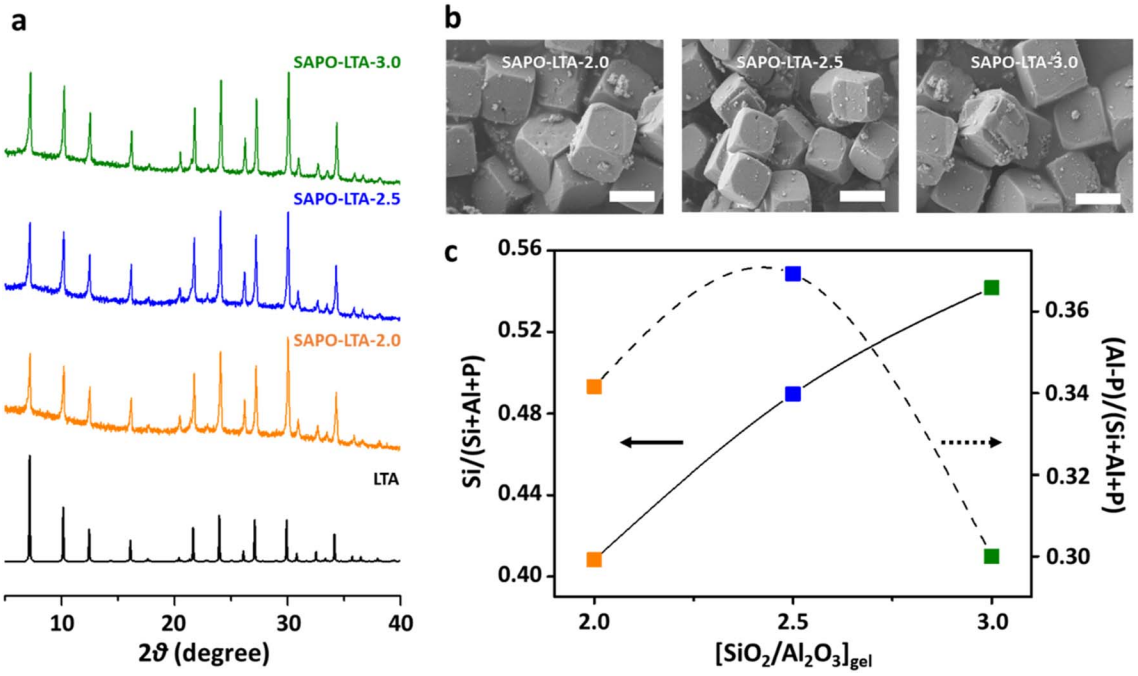

Fig. 2 Characterization of organic-free SAPO-LTA crystals with sub-micron sizes. (a) Powder XRD patterns of SAPO-LTA crystals prepared from synthesis gels with three different SiO_2/Al_2O_3 ratios (*i.e.*, 2.0, 2.5 and 3.0), which are in good agreement with the theoretical LTA pattern (bottom).[13] (b) SEM images (scale bar: 500 nm) of the SAPO-LTA crystals. (c) Framework chemical compositions of the SAPO-LTA crystals. Si/(Si + Al + P) and (Al–P)/(Si + Al + P) indicate their framework Si fraction and FCD, respectively.

 This journal is © The Royal Society of Chemistry 2025

Open Access Article. Published on 03 January 2025. Downloaded on 2/9/2026 8:08:45 PM.
This article is licensed under a Creative Commons Attribution 3.0 Unported Licence.

crystallization conditions (*i.e.*, 135 °C for 1 day) using the same SAPO gel that was already optimized for the seed synthesis.

The chemical compositions of three different SAPO-LTA crystals (size: ~500 nm) were determined by elemental and thermal analyses (Table S2 and Fig. S4†). The framework Si fraction of the SAPO materials, *i.e.*, Si/(Si + Al + P), increased with respect to the SiO_2/Al_2O_3 ratio in the gels. However, SAPO-LTA-2.5 possessed the highest FCD (the fraction of Si atoms carrying the actual charges compensated by extra-framework Na^+ cations; (Al–P)/(Si + Al + P) = 0.37), among the SAPO-LTA crystals, despite its lower Si fraction (0.49) compared to SAPO-LTA-3.0 (0.54), as shown in Fig. 2c. This is probably due to more isomorphous Si substitution for Al–P pairs according to the known Si substitution mechanism (SM) II during the crystallization, leading to the formation of a larger siliceous area within SAPO-LTA-3.0 compared to SAPO-LTA-2.5, as further evidenced by ^{29}Si MAS NMR spectroscopy (Fig. S5†).[24,25] The most abundant presence of ^{29}Si NMR resonances in the region below −90 ppm, assignable to the framework $Si(OAl)_n$ species (n = 3–0) in SAPO-LTA-3.0, indicated that its highest Si fraction rather resulted in the lowest FCD, according to charge-density matching between the anionic framework and extra-framework Na^+ cations.[26,27] This is further evidenced by the proportional decrease in the number of extra-framework Na^+ cations per unit cell as the FCD of SAPO materials decreases (Table S2†). Accordingly, the highest Na^+ concentration observed in SAPO-LTA-2.5 can be attributed to the preferential substitution of P by Si atoms over Al–P pairs (following SM I),24,25 resulting in a larger number of negatively charged Si atoms per unit cell (FCD).

^{27}Al MAS NMR spectra of all SAPO-LTA materials are characterized by a predominant resonance at 62 ppm with a small shoulder in the upfield range (30–50 ppm), assignable to tetrahedrally coordinated framework Al species under Si-rich and P-rich environments, respectively.[28] For example, SAPO-LTA-2.0 with the lowest Si fraction shows a notable presence of the ^{27}Al resonance at a lower chemical shift. Like the cases of other zeotype materials,[23,26,28] the ^{31}P MAS NMR spectra of our SAPO materials also show intense and sharp resonances around −20 ppm, indicating that most of the P atoms are also incorporated into frameworks together with Al and Si species, resulting in the successful crystallization of SAPO molecular sieves (Table S2 and Fig. S5†).

Using both SAPO-LTA crystals with different FCDs as seeds and their synthesis mixtures as secondary membrane growth media, we finally prepared SAPO-LTA-x membranes (where x is the gel SiO_2/Al_2O_3 ratio = 2.0, 2.5 or 3.0) with a typical thickness of ~20 μm (Fig. 3a and S6†). The chemical compositions of solid products obtained together with the membranes from their secondary growth mixtures further supported that the FCD of

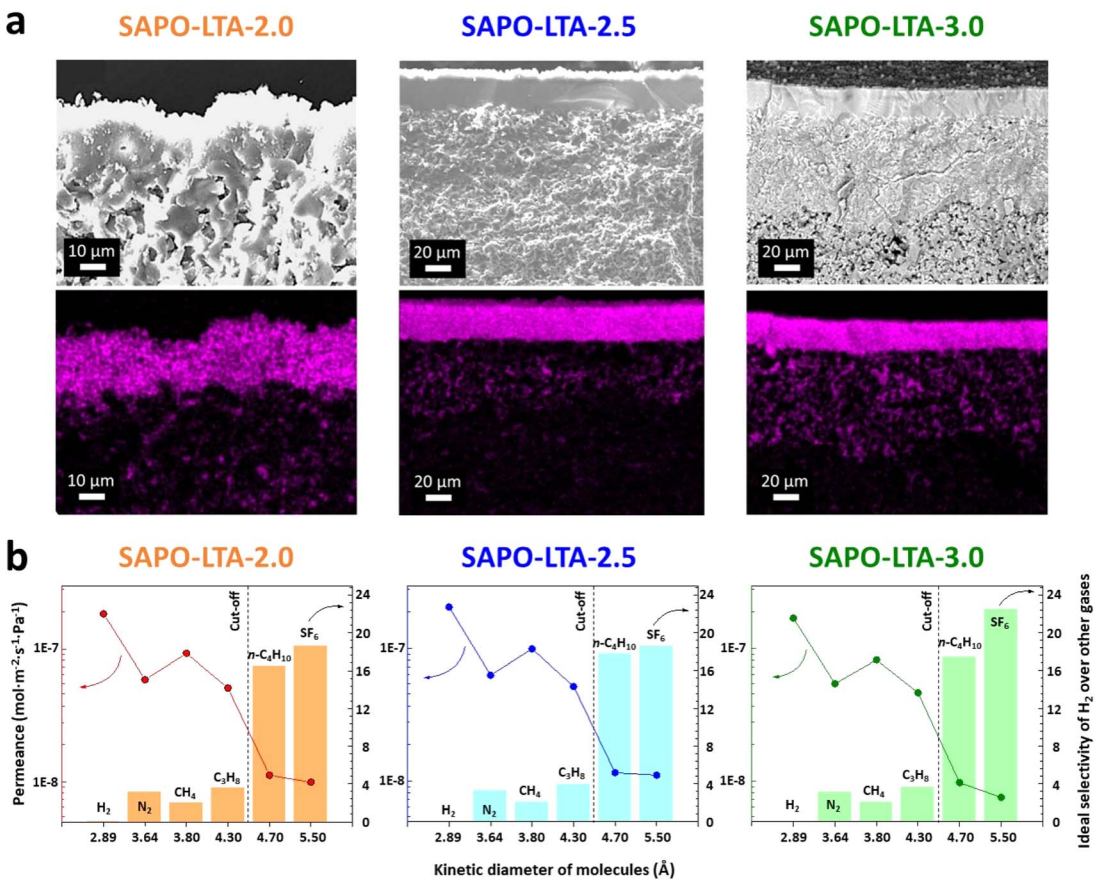

Fig. 3 SEM images and single-gas permeation of SAPO-LTA membranes. (a) SEM (top) and energy dispersive spectroscopy (bottom, Si: pink) images of SAPO-LTA membranes prepared in this work. (b) The single-gas permeance of molecules with varied kinetic diameters.

Open Access Article. Published on 03 January 2025. Downloaded on 2/9/2026 8:08:45 PM.
This article is licensed under a Creative Commons Attribution 3.0 Unported Licence.

the prepared membranes was highly likely tuned to correspond to those of the seed crystals employed in their fabrication (Table S3†).

To probe the pore sizes of our SAPO-LTA membranes, the single-gas permeation of molecules with different kinetic diameters from 2.89 to 5.50 Å was evaluated at room temperature, as shown in Fig. 3b, using a home-built dead-ended permeation system (Fig. S7†). Although it was observed that N_2 (3.64 Å) was not readily adsorbed on SAPO-LTA crystals at 77 K like the other Na^+ forms of zeolite LTA (Table S2†),[29,30] the gas molecules smaller than 4.4 Å showed a relatively small and gradual decrease for all membranes, with a permeance of 0.5–2.0 $\times 10^{-7}$ mol m^{-2} s^{-1} Pa^{-1}. However, a significant decrease in gas permeance was observed for the molecules larger than 4.6 Å, exhibiting a sharp permeance cut-off between propane and *n*-butane. Although the permeation of the large molecules was not completely inhibited, indicating the inevitable presence of a few inter-crystalline defects, the notable changes between the ideal selectivity (ratio of pure gas permeances) of H_2 over propane and *n*-butane indicated that the effective pore size of our membranes was likely ~4.5 Å, which is slightly larger than that (~4 Å) of the LTA-type $AlPO_4$ membrane.[31] This is probably due to the presence of longer Si–O bonds (bond length = 1.6 Å) in the SAPO frameworks that substituted shorter P–O bonds (1.5 Å) of the LTA-type $AlPO_4$ network, like the case of a SAPO-34 membrane with high Si incorporation.[16,32]

Of particular interest, a polar molecule, NH_3, showed considerably lower permeance at room temperature for our small-pore SAPO membranes, compared not only to non-polar H_2 of similar size, but also to N_2, which is even heavier than NH_3 (Fig. S8†). Moreover, the NH_3 permeance was found to be lower for the membrane with higher FCD. For example, the SAPO-LTA-2.5 membrane with the highest FCD of 0.37 had the lowest NH_3 permeance of 0.24 $\times 10^{-7}$ mol m^{-2} s^{-1} Pa^{-1}, while the SAPO-LTA-3.0 membrane with the lowest FCD showed about two times higher NH_3 permeance (0.43 $\times 10^{-7}$ mol m^{-2} s^{-1} Pa^{-1}). This suggests that the extent of NH_3 adsorption that may impede its diffusion through the small-pore membranes can be varied with respect to the FCD of membranes that determines their overall polar properties.

Subsequently, the effect of membrane FCD on the NH_3 separation from a mixture of $NH_3/N_2/H_2$ (molar ratio of 10.0 : 22.5 : 67.5) was further investigated at an elevated temperature of 150 °C, using a Wicke–Kallenbach system (Fig. S9†). The mixture composition is representative of a product stream of the Harber–Bosch process.[33,34] Although it was only 10 mol% in the mixture, the presence of NH_3 in the mixture sufficiently lowered the permeance of both N_2 and H_2, which otherwise had higher single-gas permeances (Fig. 4). Indeed, despite the exothermic nature of adsorption that often lowers the selectivity of membranes relying on preferential sorption in separation at elevated temperatures, the SAPO-LTA membranes showed effective NH_3 selectivity at this high temperature. Particularly, the SAPO-LTA-2.5 membrane exhibited a stronger NH_3 affinity, evidenced by the highest NH_3/N_2 and NH_3/H_2 selectivity (32.5 and 9.9, respectively), compared to other SAPO-LTA membranes having lower FCDs. Further, the NH_3 permeance (0.56 $\times 10^{-7}$ mol m^{-2} s^{-1} Pa^{-1}) of SAPO-LTA-2.5 was comparable to that of the other LTA-type zeolite membranes that are ~4 times thinner (Table S4†).[33,34] As expected, the SAPO-LTA-3.0 membrane showed the highest NH_3 permeance, as its weaker NH_3 affinity allowed a faster transport of NH_3 but failed to considerably block the permeance of the non-polar gases, resulting in the lowest NH_3 selectivity. Even at 300 °C, the SAPO-LTA-2.5 membrane maintained an adequate NH_3 separation performance with an NH_3/N_2 selectivity of 14.3 and NH_3 permeance of 0.49 $\times 10^{-7}$ mol m^{-2} s^{-1} Pa^{-1} (Fig. S10†). It is reported that to achieve *in situ* NH_3 removal in membrane reactors during NH_3 synthesis, a membrane with NH_3/N_2 selectivity >10 and NH_3 permeance >0.4 $\times 10^{-7}$ mol m^{-2} s^{-1} Pa^{-1} at 300 °C is required to make the NH_3 synthesis membrane reactor more economical compared to traditional reactors.[35] Indeed, our SAPO-LTA-2.5 membrane meets these criteria.

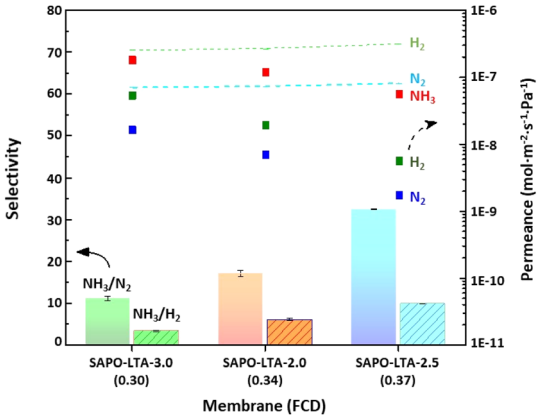

Fig. 4 Adsorption-dependent separation of NH_3 at 150 °C using SAPO-LTA membranes with different FCDs. The NH_3 selectivity (bar) over N_2 (left) and H_2 (right) of the SAPO-LTA membranes is shown with respect to their FCD. The mixture-gas permeances (symbol: ■, color code: NH_3, red; H_2, olive; N_2, blue) are compared with the single-gas permeances (dashed line, color code: H_2, green; N_2, cyan) at 150 °C.

Despite the fact that the extra-framework Na^+ cations are the predominant, if not the only, weak Lewis acid (LA) sites for NH_3 chemisorption within our organic-free SAPO materials,[36–39] NH_3-TPD profiles demonstrate that NH_3 can be effectively adsorbed on the SAPO materials up to 300 °C (Fig. S11†). The primary desorption peak consistently observed around 250 °C from SAPO-LTAs further supports the lack of strong Brønsted acid sites, such as bridging hydroxyl (Si–OH–Al) groups.[36,39] This observation also indicates that the LA strength of our LTA-type SAPO materials is nearly similar. However, the different NH_3 affinities observed in SAPO-LTA membranes are not correlated with LA strength, nor are they strictly correlated with the heat of adsorption (Fig. S12†). Interestingly, the total amount of NH_3 desorbed, derived from the NH_3-TPD desorption area, was found to be 20% and 11% larger for SAPO-LTA-2.5 (1.38 mmol g^{-1}) compared to SAPO-LTA-3.0 (1.15) and SAPO-LTA-2.0 (1.24), respectively, closely proportional to the difference in their FCDs. Given that the LA density differentiating the overall acidity of our SAPO materials essentially corresponds to the number of Na^+ cations per unit cell (Table S2†), the highest NH_3

 This journal is © The Royal Society of Chemistry 2025

Open Access Article. Published on 03 January 2025. Downloaded on 2/9/2026 8:08:45 PM.
This article is licensed under a Creative Commons Attribution 3.0 Unported Licence.

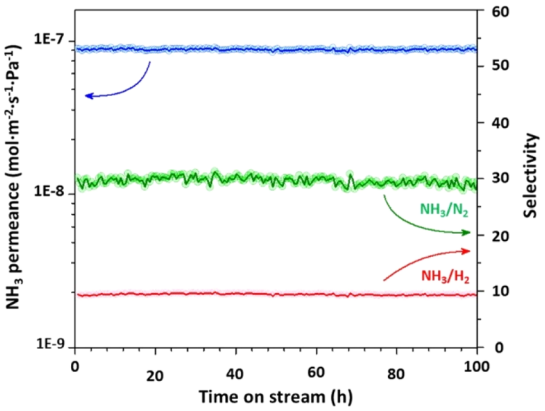

Fig. 5 A long-term (>100 h) thermal stability (at 150 °C) testing result of the SAPO-LTA-2.5 membrane for NH_3 separation.

affinity observed from the SAPO-LTA-2.5 membrane can be rationalized by its highest FCD.

We envision the use of SAPO-LTA membranes for the separation of NH_3 from unreacted N_2 and H_2 coming out of the NH_3 synthesis reactor at high temperatures. Since SAPO-LTA membranes can separate NH_3 from the mixture at high temperature, a hot retentate gas stream rich in N_2 and H_2 can be recycled back to the reactor, eliminating the need for reheating them (Fig. S13†). Indeed, to be a promising candidate for such an industrial application, membranes require long-term stability. The SAPO-LTA-2.5 membrane with the highest NH_3/N_2 selectivity at 150 °C showed excellent long-term (>100 h) thermal stability with a fluctuation of less than 5% in NH_3 separation performance (Fig. 5). These SAPO-LTA membranes are among the highest performing zeolite membranes that are reported for this challenging NH_3 separation at high temperatures (>100 °C) (Table S4†). With the opportunity to further optimize the synthesis toward thinner membranes, it would also be possible to boost the performance of organic-free SAPO membranes for other preferential adsorbent-mediated separations at elevated temperatures.

4. Conclusions

In summary, we have successfully synthesized small-pore LTA-type SAPO membranes with tunable FCD without the use of organic components. By employing Na^+ cations as an inorganic SDA in diluted SAPO synthesis mixtures with varied Si concentrations, SAPO-LTA molecular sieves with subtly adjusted FCD were prepared as seed crystals. The use of the optimized seed-synthesis mixtures as secondary membrane growth media allowed the fabrication of small-pore (~4.5 Å) SAPO-LTA membranes with tunable FCD corresponding to that of each seed crystal employed. Among the prepared membranes, that with the highest FCD and thus with the largest number of LA sites (*i.e.*, Na^+ cations) per unit cell demonstrated the highest NH_3 selectivity over N_2 (32.5) and H_2 (9.9) over 100 h at 150 °C, with an NH_3 permeance of 0.56×10^{-7} mol m^{-2} s^{-1} Pa^{-1}. The organic-free synthesis strategy presented in this work might also allow the fabrication of different types of zeotype membranes with highly charged frameworks for affinity-based separations at elevated temperatures.

Data availability

The authors confirm that the data supporting the findings of this study are available within the article and its ESI.†

Author contribution

S. H. P.: conceptualization, methodology, investigation, writing – original draft and writing – review & editing. B. S.: methodology, investigation, writing – original draft and writing – review & editing. S. E. G.: formal analysis. K. F.: investigations and formal analysis. R. L.: methodology. A. F. M. I.: investigation and formal analysis. M. Y.: supervision, funding acquisition, project administration, writing – original draft and writing – review & editing.

Conflicts of interest

The authors declare no conflicts of interest.

Acknowledgements

We thank the Advanced Research Projects Agency-Energy (ARPA-E) of Department of Energy (DOE) for the financial support under the contract of DE-AR0001479.

Notes and references

1 H. Li, C. Qiu, S. Ren, Q. Dong, S. Zhang, F. Zhou, X. Liang, J. Wang, S. Li and M. Yu, *Science*, 2020, **367**, 667.
2 B. Sengupta, Q. Dong, R. Khadka, D. Behera, R. Yang, J. Liu, J. Jiang, P. Keblinski, G. Belfort and M. Yu, *Science*, 2023, **381**, 1098.
3 X. Wu, T. Chen, G. Dong, M. Tian, J. Wang, R. Zhang, G. Zhang, J. Zhu and Y. Zhang, *Desalination*, 2024, 117379.
4 M. E. Davis, *Nature*, 2002, **417**, 813.
5 M. Yu, R. D. Noble and J. L. Falconer, *Acc. Chem. Res.*, 2011, **44**, 1196.
6 J. Gascon, F. Kapteijn, B. Zornoza, V. Sebastián, C. Casado and J. Coronas, *Chem. Mater.*, 2012, **24**, 2829.
7 N. Kosinov, J. Gascon, F. Kapteijn and E. J. M. Hensen, *J. Membr. Sci.*, 2016, **499**, 65.
8 C. Algieri and E. Drioli, *Sep. Purif. Technol.*, 2022, **278**, 119295.
9 S. T. Wilson, B. M. Lok, C. A. Messina, T. R. Cannan and E. M. Flanigen, *J. Am. Chem. Soc.*, 1982, **104**, 1146.
10 B. M. Lok, C. A. Messina, R. L. Patton, R. J. Gajek, T. R. Cannan and E. M. Flanigen, *J. Am. Chem. Soc.*, 1984, **106**, 6092.
11 C. Feng, K. C. Khulbe, T. Matsuura, R. Farnood and A. F. Ismail, *J. Membr. Sci. Res.*, 2015, **1**, 49.
12 R. Bedard and C. Liu, *Annu. Rev. Mater. Res.*, 2018, **48**, 83.

Open Access Article. Published on 03 January 2025. Downloaded on 2/9/2026 8:08:45 PM.
This article is licensed under a Creative Commons Attribution 3.0 Unported Licence.

13 Ch. Baerlocher and L. B. McCusker, *Database of zeolite structures*, **http://www.iza-structure.org/databases/**, accessed September, 2024.
14 Z. Cao, N. D. Anjikar and S. Yang, *Separations*, 2022, **9**, 47.
15 C. Ji, Y. Tian, Y. Li and Y. Lin, *Microporous Mesoporous Mater.*, 2014, **186**, 80.
16 Y. Huang, L. Wang, Z. Song, S. Li and M. Yu, *Angew. Chem.*, 2015, **127**, 10993.
17 S. Li, Z. Zong, S. J. Zhou, Y. Huang, Z. Song, X. Feng, R. Zhou, H. S. Meyer, M. Yu and M. A. Carreon, *J. Membr. Sci.*, 2015, **487**, 141.
18 H. Shi, *RSC Adv.*, 2015, **5**, 38330.
19 Q. T. Le, D. H-P Nguyen, N. M. Nguyen, D. P.-H. Nguyen, T. M. Nguyen, T. N. Nguyen and T. C. T. Pham, *ChemSusChem*, 2020, **13**, 1720.
20 B. Wang, C. Sun, R. Zhou and W. Xing, *Chem. Eng. J.*, 2022, **442**, 136336.
21 E. M. Flanigen, R. W. Broach and S. T. Wilson, in *Zeolites in Industrial Separation and Catalysis*, ed. S. Kulprathipanja, Wiley-VCH Verlag GmbH & Co. KGaA, Weinheim, Germany, 2010, ch. 1, pp. 1–26.
22 E. Pérez-Botella, S. Valencia and F. Rey, *Chem. Rev.*, 2022, **122**, 17647.
23 S. H. Park, K. C. Kemp, J. Hong, J. G. Min and S. B. Hong, *Chem. Sci.*, 2021, **12**, 10371.
24 E. M. Flanigen, R. L. Patton and S. T. Wilson, Structural, synthetic and physicochemical concepts in aluminophosphate-based molecular sieves, *Stud. Surf. Sci. Catal.*, 1988, **37**, 13–27.
25 R. Vomscheid, M. Briend, M. J. Peltre, P. P. Man and D. Barthomeuf, *J. Phys. Chem.*, 1994, **98**, 9614.
26 S. H. Park, W. Choi, H. J. Choi and S. B. Hong, *Angew. Chem., Int. Ed.*, 2018, **57**, 9413.
27 S. Seo, N. H. Ahn, J. H. Lee, L. M. Knight, J. G. Moscoso, W. A. Sinkler, S. Prabhakar, C. P. Nicholas, S. B. Hong and G. J. Lewis, *Angew. Chem., Int. Ed.*, 2019, **58**, 9032.
28 D. Hasha, L. Sierra de Saldarriaga, C. Saldarriaga, P. E. Hathaway, D. F. Cox and M. E. Davis, *J. Am. Chem. Soc.*, 1988, **110**, 2127.
29 N. Kuanchertchoo, R. Suwanpreedee, S. Kulprathipanja, P. Aungkavattana, D. Atong, K. Hemra, T. Rirksomboon and S. Wongkasemjit, *Appl. Organomet. Chem.*, 2007, **21**, 841.
30 L. Liu, R. Singh, P. Xiao, P. A. Webley and Y. Zhai, *Adsorption*, 2011, **17**, 795.
31 A. Huang, F. Liang, F. Steinbach, T. M. Gesing and J. Caro, *J. Am. Chem. Soc.*, 2010, **132**, 2140.
32 R. D. Shannon, *Acta Crystallogr. A*, 1976, **32**, 751.
33 S. Padinjarekutt, H. Li, S. Ren, P. Ramesh, F. Zhou, S. Li, G. Belfort and M. Yu, *Chem. Eng. J.*, 2023, **454**, 139998.
34 S. Padinjarekutt, B. Sengupta, H. Li, K. Friedman, D. Behera, R. Lecaros and M. Yu, *J. Membr. Sci.*, 2023, **674**, 121512.
35 Z. Zhang, J. D. Way and C. A. Wolden, *AIChE J.*, 2021, **67**(8), e17259.
36 M. Huang, S. Kaliaguine and A. Auroux, *Stud. Surf. Sci. Catal.*, 1995, **97**, 311.
37 M. Huang, A. Auroux and S. Kaliaguine, *J. Phys. Chem.*, 1995, **99**, 9952.
38 M. C. Abello, A. P. Velasco, M. F. Gomez and J. B. Rivarola, *Langmuir*, 1997, **13**, 2596.
39 M. Takeuchi, T. Tsukamoto, A. Kondo and M. Matsuoka, *Catal. Sci. Technol.*, 2015, **5**, 4587.

This journal is © The Royal Society of Chemistry 2025